2011 IEEE Intelligent Vehicles Symposium (IV)
Baden-Baden, Germany, June 5-9, 2011

Empirical Evaluation of Vehicular Models for Ego Motion Estimation

Robin Schubert, Christian Adam, Marcus Obst, Norman Mattern, Veit Leonhardt, and Gerd Wanielik

***Abstract*— Estimating the motion of a vehicle is a crucial requirement for intelligent vehicles. In order to solve this problem using a Bayes filter, an appropriate model of vehicular motions is required. This paper systematically reviews typical vehicular motion models and evaluates their suitability in different scenarios. For that, the results of extensive experiments using accurate reference sensors are presented and discussed in order to provide guidelines for the choice of an optimal model.**

I. INTRODUCTION

One of the most promising technologies for increasing road safety and driving comfort are advanced driver assistance systems (ADASs). Such systems are characterized by the perception of a vehicle's surrounding using different, often complementary sensors. In order to bridge the gap between the inherent uncertainties of the sensor measurements and the required reliability of the desired information, it is common to apply statistical signal processing techniques.

One of the most widely used concepts is the Bayes filter or, more precisely, one of its practical implementations. Each Bayes filter, however, requires an appropriate probabilistic state space model of the system under consideration which consists of two parts: While the system or process model describes the temporal behavior, the sensor model characterizes the properties of the utilized sensors [1].

For vehicular applications, a system model which accurately represents the motion of a vehicle is often a crucial requirement. While this is rather obvious for applications which explicitly address the estimation of a vehicle's motion (e.g., systems for localizing the ego vehicle [2] or tracking vehicles in the surrounding [3]), it is also true for non-vehicular tracking applications. For instance, pedestrian detection systems require an accurate ego motion estimation in order to distinguish the motions of the pedestrians from those of the ego vehicle [4].

Consequently, ego motion estimation is a part of virtually any work related to the perception of a vehicle's surrounding. Though a number of different models have been proposed, a systematic empirical evaluation is rarely available. In [5], three of the most common models have been compared based on simulated data. In [6], two models have been evaluated for a mobile robot. Finally, an evaluation of sophisticated models for navigation purposes has been presented in [7].

Another related work, which was done by some of the authors, attempted to evaluate different motion models for navigation purposes using highly accurate reference sensors [8]. However, there are some factors which limit the significance of this evaluation for ADAS applications. In contrast to usual tracking algorithms, position measurements from a global navigation satellite system (GNSS) have been used. Furthermore, in lack of a more appropriate procedure, the filter parameters have been tuned manually.

In this paper, the most common vehicular motion models shall be empirically evaluated, in particular regarding their suitability for ADAS applications. The basic idea is to apply identical filters each of which contains a separate motion model using automatically optimized parameters. The experiments are conducted in different environments such as highways or urban roads using a highly accurate reference sensor system.

The paper is structured as follows: Section II introduces the utilized notation and gives a brief overview about probabilistic filtering and common motion models. In the subsequent section III, the experimental setup as well as the evaluation methodology are presented. Section IV contains detailed quantitative results of the motion model evaluation. The paper concludes with a discussion and recommendations about appropriate models in section V.

II. FUNDAMENTALS

A. Probabilistic Filtering

The aim of Bayesian tracking algorithms is to recursively estimate the probability density function (PDF) of a system's n_x-dimensional state vector $\mathbf{x}_k \in \mathbb{R}^{n_x}$ for each time step k. The dynamic behavior of the system is represented by the discrete-time stochastic model

$$\mathbf{x}_{k+1} = \mathbf{g}_a(\mathbf{x}_k, \mathbf{v}_k, T_k), \tag{1}$$

where $\mathbf{g}_a$ is called *state transition equation*. The vector $\mathbf{v}_k$ denotes an independent and identically distributed (i.i.d.) system noise process, which represents the non-deterministic part of the model. T_k denotes the time between k and $k+1$.

In the general case, the state vector $\mathbf{x}_k$ is not observable; however, it is assumed that measurements $\mathbf{y}_k \in \mathbb{R}^{n_y}$ are available which are connected to $\mathbf{x}_k$ by a known mathematical relation, called the *measurement equation*

$$\mathbf{y}_k = \mathbf{g}_c(\mathbf{x}_k, \mathbf{w}_k), \tag{2}$$

where $\mathbf{w}_k$ denotes an i.i.d. observation noise time series.

For the filtering problem, the noise processes are assumed to be white and mutually independent. Furthermore, the sequence of all measurements which are available at time k is denoted by $\mathbf{Y}_k \widehat{=} \{\mathbf{y}_i, i = 1, \ldots, k\}$. If the initial PDF $p(\mathbf{x}_0)$ is assumed to be known, the *filtering problem* can be defined as recursively determining the posterior PDF $p(\mathbf{x}_k|\mathbf{Y}_k)$.

All authors are with the Professorship of Communications Engineering, Chemnitz University of Technology, Chemnitz, Germany, e-mail: firstname.lastname@etit.tu-chemnitz.de

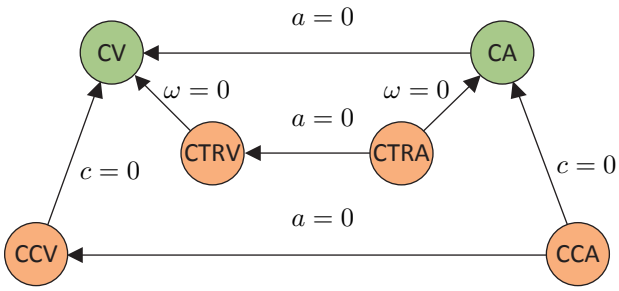

Fig. 1. Systematization of common motion models [8] which distinguishes between linear models (green) and curvilinear models (orange).

B. Vehicular Motion Models

The basic idea of any motion models is that a mass cannot move arbitrarily, but is subject to inertia. Thus, the simplest model class is based on Newton's laws of motion and assumes either a linear or a uniformly accelerated motion. Using a common nomenclature which names a model after the quantities which are assumed to be constant, the former leads to the *constant velocity* (CV) model, while the latter is called *constant acceleration* (CA). Higher derivatives (such as a constant jerk model) are not considered in this work. Due to the fact that this class of models can be described by a polynomial over time which in turn can be represented by a linear matrix projection, the term *linear models* is often applied.

Other models are extending the linear class by a rotation and are, thus, often called *curvilinear models*. The simplest form which models a constant turn rate without any explicit relation to the velocity is called *constant turn rate and velocity* (CTRV) or *constant turn rate and acceleration* (CTRA) model. An alternative representation can be obtained by exploiting the fact that a vehicle cannot turn arbitrarily, but is subject to nonholonomic constraints [9]. This is sometimes referred to as the *bicycle model*, however, for the sake of a consistent nomenclature, the term constant curvature and velocity (CCV) or constant curvature and acceleration (CCA) is used in this paper. Again, models which explicitly represent rotational accelerations will not be considered in the following.

There are also more sophisticated models which account for additional effects such as wheel slip or skidding. As such models are particularly useful in extreme driving situations, their evaluation is more challenging. Further details about such models can be found in [7], [10], [11].

In the following, the state spaces and transition equations for the evaluated models will be presented. As a general remark, it shall be noted that obviously all models are not able to describe the motion of a vehicle perfectly. Thus, each model contains a probabilistic part which is at least for Gaussian filters often modeled as an additive zero-mean noise $\mathbf{v_k}$ with given variance (see section II-A). For the sake of compactness, these noise terms are omitted in the following equations.

1) Constant Position: As a basic reference for the evaluation, all models are compared to a filter without any explicit motion model. In an abuse of language, this will be called "constant position" (CP) model. It consists of the state space ${}^{\text{CP}}\mathbf{x} = (x\ y)^T$ and the transition equation ${}^{\text{CP}}\mathbf{x}_{k+1} = {}^{\text{CP}}\mathbf{x}_k$.

2) Constant Velocity: There are two variants of this model, as the state space may contain either two velocity components in longitudinal and lateral direction or the norm of the velocity vector v and a heading angle ϑ. In this work, the latter approach has been chosen, which leads to the state space

$$ {}^{\text{CV}}\mathbf{x} = \begin{pmatrix} x & y & \vartheta & v \end{pmatrix}^{\text{T}} \tag{3} $$

and the state transition equation

$$ \mathbf{x}_{k+1} = \mathbf{x}_k + \begin{pmatrix} v\cos(\vartheta)T_k \\ v\sin(\vartheta)T_k \\ 0 \\ 0 \end{pmatrix}. \tag{4} $$

3) Constant Acceleration: This model represents a uniformly accelerated motion and is characterized by the state space

$$ {}^{\text{CA}}\mathbf{x} = \begin{pmatrix} x & y & \vartheta & v & a \end{pmatrix}^{\text{T}}. \tag{5} $$

where a denotes the longitudinal acceleration. The state transition equation is

$$ \mathbf{x}_{k+1} = \mathbf{x}_k + \begin{pmatrix} \left(v_k T_k + \frac{a}{2}T_k^2\right)\cos(\vartheta) \\ \left(v_k T_k + \frac{a}{2}T_k^2\right)\sin(\vartheta) \\ 0 \\ aT_k \\ 0 \end{pmatrix}. \tag{6} $$

4) Constant Turn Rate and Velocity: For this model, the CV state space is extended by the turn rate $\omega = \dot{\vartheta}$, i.e.,

$$ {}^{\text{CTRV}}\mathbf{x} = \begin{pmatrix} x & y & \vartheta & v & \omega \end{pmatrix}^{\text{T}}. \tag{7} $$

The state transition equation requires a case discrimination: For $\omega = 0$, equation 4 can be applied, while

$$ \mathbf{x}_{k+1} = \mathbf{x}_k + \begin{pmatrix} \frac{v}{\omega}\left[\sin(\vartheta_k + \omega T_k) - \sin(\vartheta_k)\right] \\ \frac{v}{\omega}\left[\cos(\vartheta_k) - \cos(\vartheta_k + \omega T_k)\right] \\ \omega T_k \\ 0 \\ 0 \end{pmatrix} \tag{8} $$

is required otherwise.

5) Constant Turn Rate and Acceleration: Compared to the CTRV model, the state space is extended by the acceleration $a = \dot{v}$, that is,

$$ {}^{\text{CTRA}}\mathbf{x} = \begin{pmatrix} x & y & \vartheta & v & a & \omega \end{pmatrix}^{\text{T}}. \tag{9} $$

The state transition equation can be written as

$$ \mathbf{x}_{k+1} = \mathbf{x}_k + \begin{pmatrix} g_x(\mathbf{x}_k, T_k) \\ g_y(\mathbf{x}_k, T_k) \\ \omega T_k \\ aT_k \\ 0 \\ 0 \end{pmatrix}, \tag{10} $$

where

$$g_x = \frac{a[\cos(\vartheta_k + \omega T_k) - \cos(\vartheta_k)]}{\omega^2} + \frac{(v_k + aT_k)\sin(\vartheta_k + \omega T_k) - v_k \sin(\vartheta_k)}{\omega}, \tag{11}$$

$$g_y = \frac{a[\sin(\vartheta_k + \omega T_k) - \sin(\vartheta_k)]}{\omega^2} - \frac{(v_k + aT_k)\cos(\vartheta_k + \omega T_k) - v_k \cos(\vartheta_k)}{\omega}. \tag{12}$$

6) Constant Curvature and Acceleration: This model describes an uniformly accelerated motion along a circular arc. The state space is

$${}^{\text{CCA}}\mathbf{x} = \begin{pmatrix} x & y & \vartheta & v & a & c \end{pmatrix}^{\mathrm{T}}, \tag{13}$$

where c denotes the curvature of the circular arc, which is the reciprocal value of its radius. The state transition equation is

$$\mathbf{x}_{k+1} = \mathbf{x}_k + \begin{pmatrix} \Delta x_k \cos(\vartheta_k) - \Delta y_k \sin(\vartheta_k) \\ \Delta x_k \sin(\vartheta_k) + \Delta y_k \cos(\vartheta_k) \\ b_k\, c_k \\ aT_k \\ 0 \\ 0 \end{pmatrix}, \tag{14}$$

with

$$b_k = \frac{a}{2} T_k^2 + v_k T_k \tag{15}$$

denoting the length of the covered way and Δx and Δy indicating the shift in longitudinal and lateral direction. For $c \neq 0$, this is

$$\Delta x_k = \frac{1}{c_k} \sin(b_k c_k), \tag{16}$$

$$\Delta y_k = \frac{1}{c_k} (1 - \cos(b_k c_k)). \tag{17}$$

For a straight motion, i. e. $c = 0$, the shift is

$$\Delta x_{k,c=0} = \lim_{c \to 0} \Delta x_k = b, \tag{18}$$

$$\Delta y_{k,c=0} = \lim_{c \to 0} \Delta y_k = 0. \tag{19}$$

If the acceleration is removed from the state vector and set to zero in (15), the model degenerates to a CCV model.

C. Sensor Models

In similarity to the motion models, there is also a variety of sensor models with different levels of complexity. As the main objective of this paper is to compare and evaluate motion models, the simplest sensor models have been chosen for each filter, meaning that the elements of the state vector are defined as directly observed. An exception is the CCA model, where the yaw rate is not contained in the state vector, but calculated by

$$\omega_k = v_k c_k. \tag{20}$$

More complex sensor models which account for effects such as biases, scale factors, or differences in the velocity of each wheel can be found in [12], [13].

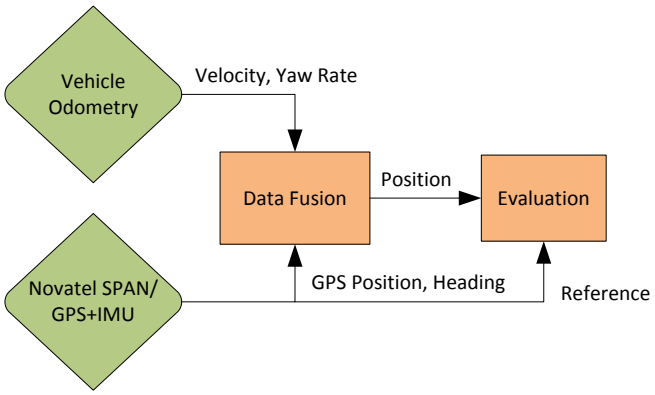

Fig. 2. Experimental setup used for the motion model evaluation. The odometry was obtained by internal vehicle sensors, while the ground truth was provided by a GPS+IMU reference system with RTK support.

III. EXPERIMENTAL SETUP

A. Sensor Configuration

In order to perform a motion model evaluation, real experimental data were recorded during several test drives using the rapid-prototyping test vehicle *Carai* [14]. The test vehicle was configured with the system setup shown in fig. 2.

The data fusion component estimates the current position of the vehicle by taking into account velocity and yaw rate measurements. These odometry measurements are obtained from the internal vehicle's controller area network (CAN) bus with a rate of 50 Hz and filtered using the vehicular motion models previously described in section II-B. The integration of the measurements and motion model is done via an implementation of the Bayesian tracking algorithm through the *Unscented Kalman Filter* (UKF) [15]. For the UKF implementation the process noise is integrated into the state space to estimate, while the observation noise is additive and constant.

Due to the latter filter optimization and evaluation a highly reliable ground truth reference is needed. A NovAtel SPAN System which integrates GNSS positioning and inertial navigation was chosen. It consists of a dual-frequency global positioning system (GPS) receiver with support for Real Time Kinematic (RTK). Together with the Honeywell HG1700 inertial measurement unit (IMU), a reliable reference trajectory with sub-decimeter accuracy is achievable. Even under difficult reception conditions, like in urban areas where full GPS satellite outages may occur, the IMU provides a stabilized ground truth for up to 10 s. Recording of ground truth trajectory was done with 50 Hz where position, attitude and velocity were considered. Additionally, the quality of the ground truth was monitored and reported if the required accuracy could not be guaranteed; such measurements were not used for the evaluation.

B. Evaluation Methodology

For this evaluation several test drives have been conducted. The routes have been chosen to reflect typical scenarios in

TABLE I

OVERVIEW OF SCENARIOS AND DRIVING DURATION FOR EVALUATION.

Scenario	Duration	Lot	Description
Urban	45:00 min	57 %	Many acceleration and braking maneuvers, roundabouts. Velocity was up to 50 km/h. Four minutes from this sequence were used for the optimization.
Suburban	10:00 min	13 %	Medium acceleration and braking maneuvers. Velocity up to 60 km/h.
Highway	24:00 min	30 %	Includes lane change maneuvers and slip roads. Velocity up to 130 km/h.

TABLE II

PROCESS AND MEASUREMENT NOISE STANDARD DEVIATIONS.

Parameter	Description	Value
σ_x, σ_y	Position process noise	6.0 m
σ_ϑ	Heading process noise	$2.3 \cdot 10^{-4}$ rad
σ_v	Velocity process noise	1.5 m/s
σ_a	Acceleration process noise	8.8 m/s^2
σ_ω	Yaw rate process noise	0.29 rad/s
σ_c	Curvature process noise	3.6 m^{-1}
$\sigma_{\text{meas},v}$	Velocity measurement noise	$4.07 \cdot 10^{-2}$ m/s
$\sigma_{\text{meas},\omega}$	Yaw rate measurement noise	$2.53 \cdot 10^{-3}$ rad/s

ADAS applications. In table I an overview of the performed scenarios and their duration for the evaluation is given. One of the main efforts during performing these test drives was to include common maneuvers like braking and accelerating in dense urban environment or lane changing on highways.

After recording the required raw data and ground truth for all scenarios, an independent automatic optimization of the UKF filter parameters (process noise) for the motion models under investigation was performed. The optimization procedure includes only a subsequence (approx. 4 minutes) of the urban test drive to mitigate interdependence between optimization and evaluation steps. In order to achieve this, different sets of process noise parameters $\mathbf{e}$ were automatically chosen by the optimizer and applied to the prior selected subsequence. Internally, the assessment of the optimal parameter set $\mathbf{e}_{\text{opt}}$ is done through maximization of the overall likelihood as fitness: $\mathbf{e}_{\text{opt}} = \arg\max f(\mathbf{e})$. This means to multiply the single likelihoods generated from evaluating the estimated state $\hat{\mathbf{x}}_k$ at the corresponding ground truth $\mathbf{x}_k$:

$$f(\mathbf{e}) = \prod_{k \in \{5,10,\ldots,n\}} p(\mathbf{x}_k | \hat{\mathbf{x}}_k), \tag{21}$$

with

$$p(\mathbf{x}_k | \hat{\mathbf{x}}_k) = \frac{1}{(2\pi)^{\frac{n_x}{2}} |\mathbf{P}|^{\frac{1}{2}}} e^{-\frac{1}{2}(\mathbf{x}_k - \hat{\mathbf{x}}_k)^{\mathrm{T}} \mathbf{P}^{-1} (\mathbf{x}_k - \hat{\mathbf{x}}_k)}. \tag{22}$$

To account for correlations between sequential estimates, only every 5th time step is considered.

Though the filters were optimized independently, the determined common filter parameters are almost identically. The parameters used are listed in table II. The measurement noise was determined by calculating the difference between ground truth and measurement. Afterwards, these parameters were used to evaluate the models with the test sequences

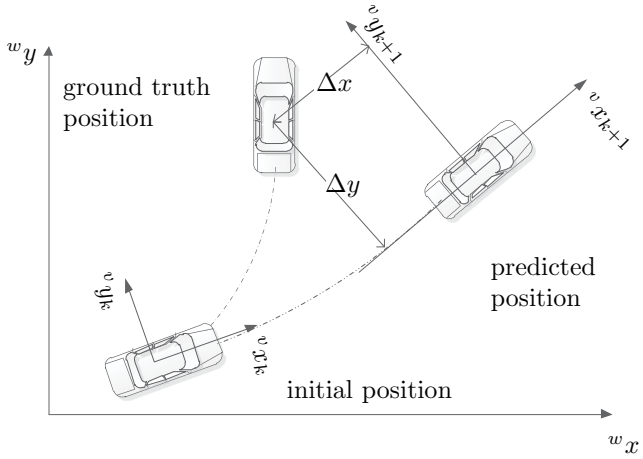

Fig. 3. Geometric representation of the evaluation process. The motion model filters are initialized at time k by the ground truth position and heading. At time $k+1$ the position deviation between the new ground truth and the predicted vehicle position is calculated in vehicle frame coordinates.

from table I. Since motion models can only predict a relative position change in time, the absolute position and heading contained in the state vector to estimate needs to be reinitialized with known values periodically (here the ground truth $\mathbf{x}$ is used). In fig. 3 the main idea of the evaluation for one period is shown:

1) At time k the initial states $(x\, y\, \vartheta)^{\mathrm{T}}$ of the motion model filter are reset to the values of the current ground truth $\mathbf{x}_k$, so that the estimated and ground truth vehicle states are aligned.
2) Up to time $k+1$ several odometry measurements are incorporated via the vehicular motion model.
3) At $k+1$ the states $(x\, y\, \vartheta)^{\mathrm{T}}$ of the new ground truth $\mathbf{x}_{k+1}$ are compared to the estimated states of $\hat{\mathbf{x}}_{k+1}$. The 2d-position difference and heading difference between ground truth and estimation are calculated in vehicle frame coordinates of the estimated position and stored for later analysis. For the CP model, the ground truth heading is used for the transformation. Thus, we obtain the position error in longitudinal (Δx) and lateral (Δy) direction. Afterwards the motion model filter is reset and the evaluation of a new period starts at step 1) again.

The time for one evaluation period was set to 80 ms.

IV. QUANTITATIVE RESULTS

A. Position error

For the comparison of the error between the estimated position of each filter and the ground truth position after one evaluation period, the 2D-position deviations of the whole test sequence were approximated by a Gaussian representation. Fig. 4 exemplarily shows the scatter plot of the CP model and its Gaussian representation. The mean value is indicated by an asterisk, the covariance ellipse shows the 3σ interval. In order to avoid distortions from long stops, e. g. at traffic lights, only samples where the vehicle was moving were considered.

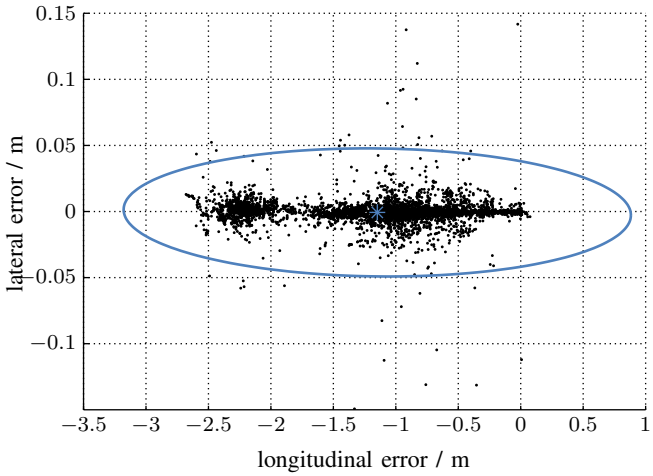

Fig. 4. Scatter plot and Gaussian approximation of the position error for the CP model over the whole test sequence. The covariance ellipse indicates the 3σ interval. For the sake of clarity, only 5000 randomly chosen samples are shown. The left bulge is caused by the highway part of the test drive, the right one by the urban part.

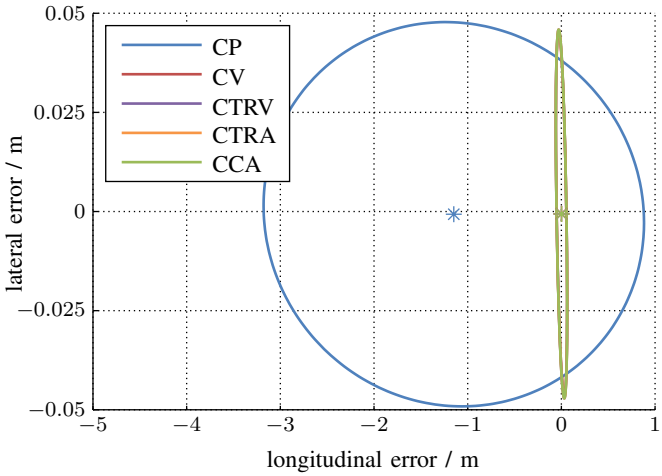

Fig. 5. Mean and covariance of position errors in longitudinal and lateral direction for 0.08 s prediction time. CV, CTRV, CTRA and CCA models are superposed. The covariance ellipse indicates the 3σ interval. The errors are slightly correlated, as the the number of turns and maneuvers to the left resp. right direction differs.

The complete time series consists of approx. 58 000 samples. Two bulges are visible in the scatter plot. The left one is caused by the highway parts of the test drive, where the velocity was around 28 m/s. The right bulge comes from the urban part with a mean velocity of 13 m/s. The area between the bulges is due to the suburban part.

The position errors of all filters are depicted in fig. 5. The mean longitudinal error of the CP model is less than zero, as its predicted position is equal to the position at the beginning of the evaluation interval and, therefore, is behind the ground truth. The estimation errors of the other filters have zero mean, as they respect the vehicles movement. Although the CV model ignores lateral movements, its lateral deviation is almost identical to the one of the curvilinear models. The reason is the short evaluation interval, wherein the actual lateral position change of a vehicle has the same magnitude as the prediction error of the curvilinear models. The reader may notice the different axis ranges in fig. 5.

When the interval between the resets is extended to one second, the insufficient heading prediction of the CV model influences clearly the lateral error (fig. 6). The lateral errors of the other models are similar. However, the CTRV and CTRA models induce a better longitudinal estimation than the CCA model. The errors are slightly correlated, depicted by the inclination of the covariance ellipse. The reason is that the direction of maneuvers and turns was not uniformly distributed during the test drive.

B. Heading and velocity error

For the calculation of the heading error, the existence of two possible difference angles must be regarded. The following equation determines the lesser difference:

$$\Delta\vartheta = \Big((\hat{\vartheta} - \vartheta + 3\pi) \mod 2\pi\Big) - \pi. \tag{23}$$

In fig. 7, the Gaussian representations of the heading errors are shown. Although the mean deviation of all filters is zero, the

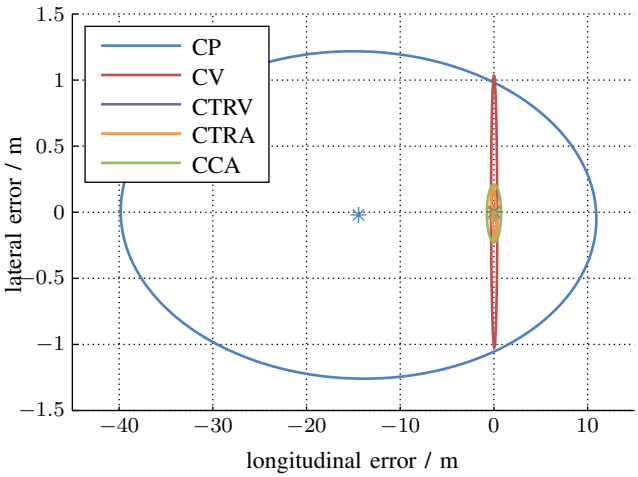

Fig. 6. Mean and covariance of position errors in longitudinal and lateral direction for 1 s prediction time. CTRV and CTRA models are superposed.

variance of the CV model is significantly larger than the one of the other models. The curvilinear models produce similar results. Due to the short evaluation interval, the different accuracies have no observable affects on the lateral position error, as already mentioned in sec. IV-A.

The errors of the estimated velocity are depicted in fig. 8. The models accounting for the acceleration produce slightly better estimation results, as the urban part of the test drive contains many acceleration maneuvers. The separate results for each scenario are very different. On urban scenario, the CTRA and CCA model have similar estimation performances, that are better than CTRV. On the other hand, on suburban routes and highways, the CTRV and CTRA are almost identical, while the CCA model shows worse behavior.

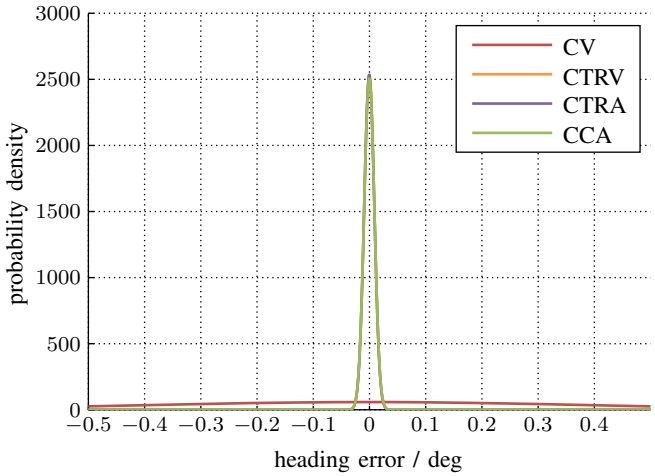

Fig. 7. Gaussian approximation of heading errors. CTRV, CTRA and CCA models are superposed; their standard deviations are 0.0090°. The standard deviation for the CV model is 0.39°.

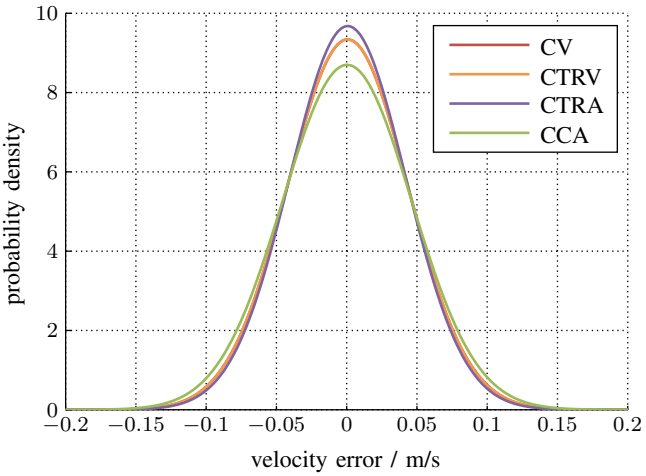

Fig. 8. Gaussian approximation of velocity errors. CV and CTRV are superposed.

V. CONCLUSIONS

This paper attempted to compare and evaluate different vehicular motion models in an experimental approach. However, it turned out that a recommendation for a certain model heavily depends on the application.

For ego motion estimation purposes which are characterized by a high update rate and the observability of v and ω, model complexities beyond CTRV do not appear to be beneficial. On the contrary, if only a position estimate is required, the CV model turned out to be surprisingly well-performing. However, the CTRV model shows its advantages as soon as a heading estimate is required.

The situation appears different if a prediction for a longer period of time is required (see fig. 6). This is indeed of practical relevance, for instance if a time to collision with respect to another vehicle or a time to lane crossing is to be estimated. In such cases, complex models can indeed improve the estimation accuracy.

Due to the improved evaluation methodology, these results refine the conclusions drawn in [8]. While the main statement of [8] was that an increasing model complexity is beneficial up to the CTRA model, it could be empirically shown in this work that an appropriate model choice depends on different factors such as the scenario, the observability of motion parameters, and the required prediction interval.

Other questions which must remain unanswered at this time include whether a more accurate ego motion estimation indeed improves the performance of tracking applications. This issue will be the subject of further work by the authors.

ACKNOWLEDGMENT

For this evaluation and generation of ground truth data, precise real-time corrections provided by the ascos service (http://www.ascos.de) were used.

REFERENCES

[1] S. Thrun, W. Burgard, and D. Fox, *Probabilistic Robotics*. The MIT Press, 2005.

[2] N. Mattern, R. Schubert, and G. Wanielik, "High-accurate vehicle localization using digital maps and coherency images," in *Proceedings of the IEEE Intelligent Vehicles Symposium*, 2010, pp. 462–469.

[3] M. Mählisch, R. Hering, W. Ritter, and K. Dietmayer, "Heterogeneous Fusion of Video, LIDAR and ESP Data for Automotive ACC Vehicle Tracking," in *Proceedings of the IEEE International Conference on Multisensor Fusion and Integration for Intelligent Systems*, 2006, pp. 139–144.

[4] B. Fardi, I. Seifert, G. Wanielik, and J. Gayko, "Motion-based pedestrian recognition from a moving vehicle," in *Proceedings of the IEEE Intelligent Vehicles Symposium*, 2006, pp. 219–224.

[5] M. Tsogas, A. Polychronopoulos, and A. Amditis, "Unscented Kalman Filter Design for Curvilinear Motion Models Suitable for Automotive Safety Applications," in *Proceedings of the 8th International Conference on Information Fusion*, 2005, pp. 1295–1302.

[6] T. Quyen Bui and K.-S. Hong, "A comparison of using probabilistic motion models for mobile robot pose estimation," in *ICCAS-SICE*, 2009, pp. 528–532.

[7] S. Julier and H. Durrant-Whyte, "On the role of process models in autonomous land vehicle navigation systems," *Robotics and Automation, IEEE Transactions on*, vol. 19, no. 1, pp. 1–14, Feb. 2003.

[8] R. Schubert, E. Richter, and G. Wanielik, "Comparison and evaluation of advanced motion models for vehicle tracking," in *Proceedings of the 11th International Conference on Information Fusion*, 2008.

[9] S. M. Lavalle, *Planning Algorithms*, 1st ed. Cambridge University Press, June 2006. [Online]. Available: http://msl.cs.uiuc.edu/planning/

[10] R. Pepy, A. Lambert, and H. Mounier, "Reducing Navigation Errors by Planning with Realistic Vehicle Model," in *Proceedings of the IEEE Intelligent Vehicles Symposium*, 2006, pp. 300–307.

[11] T. Weiss, S. Wender, and K. Dietmayer, "Landmark Navigation for Robust Object Tracking in Skidding Maneuvers Using Laser Scanners," in *Advanced Microsystems for Automotive Applications 2007*, J. Valldorf and W. Gessner, Eds. Springer Berlin Heidelberg, 2007, pp. 99–118.

[12] J. Ackermann, "Robust control prevents car skidding," *IEEE Control Systems Magazine*, vol. 17, no. 3, pp. 23–31, June 1997.

[13] M. Mählisch, "Filtersynthese zur simultanen Minimierung von Existenz-Assoziations- und Zustandsunsicherheiten in der Fahrzeugumfelderfassung mit heterogenen Sensordaten," Ph.D. dissertation, Ulm University, 2009, In German.

[14] R. Schubert, E. Richter, N. Mattern, P. Lindner, and G. Wanielik, *Advanced Microsystems for Automotive Applications 2010*. Springer, 2010, ch. A Concept Vehicle for Rapid Prototyping of Advanced Driver Assistance Systems, pp. 211–219.

[15] S. J. Julier and J. K. Uhlmann, "Unscented filtering and nonlinear estimation," *Proceedings of the IEEE*, vol. 92, no. 3, pp. 401–422, March 2004.